Cold Regions Science and Technology 131 (2016) 116–128

Contents lists available at ScienceDirect

Cold Regions Science and Technology

journal homepage: www.elsevier.com/locate/coldregions

River ice monitoring with MODIS: Application over Lower Susquehanna River

S. Kraatz *, R. Khanbilvardi, P. Romanov

NOAA-CREST Institute, The City University of New York, New York, NY, USA

ARTICLE INFO

Article history:
Received 16 January 2016
Received in revised form 11 July 2016
Accepted 10 September 2016
Available online 14 September 2016

Keywords:
River ice
Modis
Cloud mask
Susquehanna
Remote sensing

ABSTRACT

Spatially detailed characterization of the distribution, amount and timing of river ice is important for identifying and predicting potential ice hazards. Although information on the ice cover over inland water bodies is provided within MODIS snow products (MOD10 and MYD10), this information has little practical value for river ice monitoring. First, many rivers are not properly resolved in the MODIS land/water mask. Second, the cloud mask incorporated in the product is conservative and therefore results in reduced effective area coverage of the product. Third, the accuracy of the incorporated cloud mask (MOD35) depends on the particular setting and underlying land/water mask. The MODIS cloud mask is not suitable for this particular setting, if frequent ice observations are desired.

In this study we present an alternative river ice monitoring algorithm for MODIS that identifies river ice both in cloud-free conditions and through some semitransparent clouds. As input the semitransparent cloud algorithm (STC) uses an improved land/water mask accurately delineating the river channel along with bands 4 and 7 data from the MODIS surface reflectance product. The algorithm was developed for the MODIS instrument and comprehensively tested with MODIS Aqua data over the Lower Susquehanna River for the 2014 winter season. It is shown that river ice cover retrievals made with STC are highly consistent with in situ observed ice processes, for both individual scenes and the overall winter period. Owing to a better-suited cloud masking algorithm, the new technique yields nearly twice as many usable river observations during the ice-bearing period as compared to the MODIS cloud cover product. The presented approach provides potential for more timely identification of river ice changes and hence more accurate prediction of ice-related hazards using MODIS data.

1. Introduction

Springtime floods on large rivers in cold regions are a well-known serious hazard. Flood severity typically increases with discharge (Beltaos and Prowse, 2001). Spring floods are often caused by ice jams. Ice jams may stay in place for several days and back up ice for 10's of kilometers (EIJ, 2013; Newsminer, 2013). To predict ice jams and thus to minimize damages related to floods, accurate and timely information on the state of the river ice cover and on the river ice distribution along the river channel are needed.

Because of the lack of an established quality controlled network of river ice observations and the low density of hydrometric stations, operational hydrologists have to rely on in situ observations of river ice made mostly by volunteer observers.

Owing to up to 250 m, spatial resolution information provided by optical imaging instruments onboard modern meteorological polar-orbiting satellites these observations can be used for ice monitoring on large rivers. Due to daily revisit time period meteorological satellites can complement in situ and airborne observations of ice and be used to improve estimates of river ice over large regions (Chaouch et al., 2012; Pavelsky and Smith, 2004). Ice over inland water bodies, including large rivers is incorporated in the snow cover products derived with the Moderate Resolution Imaging Spectroradiometer (MODIS) onboard Aqua and Terra satellites (Hall et al., 2002) and with the Visible Infrared Imaging Radiometer Suite (VIIRS) onboard S-NPP and future JPSS satellites (Baker, 2011).

Satellite-based ice monitoring from observations in the visible and infrared spectral bands is complicated by clouds which are mostly opaque at these wavelengths. Persistent cloud cover hampers the ability to timely characterize changes in the river ice distribution and prevents timely identification of ice jams. Furthermore, the cloud masking algorithms incorporated both in the MODIS and VIIRS data processing systems are global and therefore may not be optimal for certain small geographical regions of the size of a river watershed. A number of papers reported on noticeable overestimations, false alarms and biases of the cloud amount by the MODIS cloud mask (Hall and Riggs, 2007; Maddux et al., 2010; Wilson et al., 2014). Because of limitations of the

* Corresponding author.
E-mail address: skraatz00@citymail.cuny.edu (S. Kraatz).

http://dx.doi.org/10.1016/j.coldregions.2016.09.012
0165-232X/

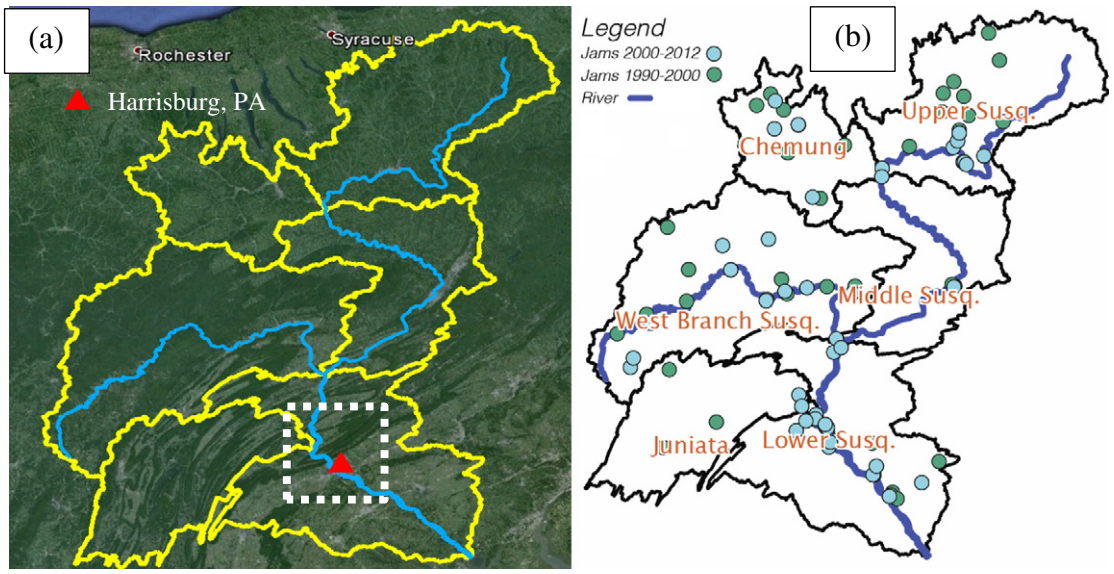

Fig. 1. (a) Susquehanna River (blue) with major basins (yellow) and the region of interest (dotted square) on Google Earth and (b) Susquehanna River with major basins and past jams (CRREL IJDB).

MODIS cloud mask specific to snow, Sirguey et al. (2009) replaced the MODIS global cloud mask with a locally-adjusted cloud identification algorithm which provided more accurate and realistic characterization of cloud cover (Sirguey et al., 2009). Also, in part due to limitations with cloud products, the operational VIIRS flood map product, available through the RealEarth project website operated by University of Wisconsin (http://realearth.ssec.wisc.edu/) has its own cloud identification algorithm (Li, 2013). It has since been replaced by a VIIRS cloud mask which underestimates cloud cover compared to MODIS. We came to similar conclusions while qualitatively examining the MODIS snow and cloud cover products and evaluating their ability to characterize river ice cover (Kraatz et al., 2015). We found that the MODIS cloud mask tends to overestimate clouds over the river, in particular when riverbanks are snow covered and the river bears ice. These factors were found to significantly reduce clear-sky river observations especially when river ice is present.

Past attempts to routinely map and monitor river ice cover with satellite data have been reported. Pavelsky and Smith (2004) used the Advanced Very High Resolution Radiometer (AVHRR) and MODIS to examine the ice break-up on large arctic rivers over ten years, and employed a visual identification approach to distinguish between water and ice. Chaouch et al. (2012) developed a MODIS-based algorithm to identify ice on large rivers. It has been incorporated in the CREST River Ice Observing System (CRIOS) to automatically detect river ice within the Susquehanna Basins and uses a threshold-based decision tree to classify between land, water, ice and mixed grid cells. CRIOS was evaluated using aerial imagery, lake ice recording and achieved a 91% probability of ice detection when compared to Landsat. The algorithm has since been modified and applied to VIIRS and applied to several large river basins in the US with images available through the RealEarth project website. It is important to note that CRIOS relies on the standard MODIS cloud mask for cloud identification. As result, the effective daily area coverage of the product may be substantially reduced due to cloud overestimation. Muhammad et al. (2015) used Terra and Aqua snow and radiance products to monitor ice break-up on the Mackenzie River. The temporal coverage was improved by applying threshold-based classification of MODIS radiances where the cloud mask based snow products indicated clouds.

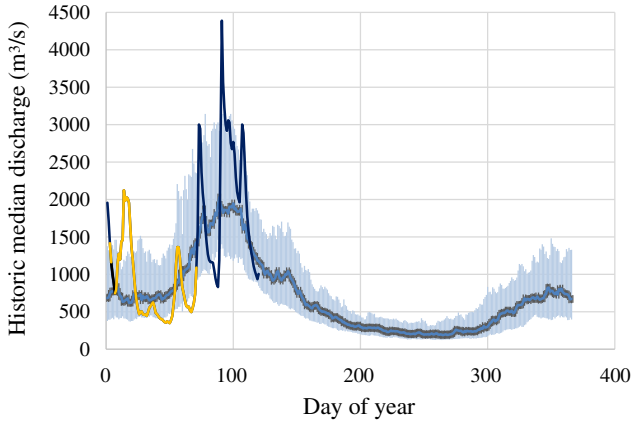

Fig. 2. Shown in blue is the 125-year median discharge with the shaded region indicating the range of 25th and 75th percentile flows at Harrisburg, PA. Shown in black are the daily average flows for Nov 1, 2013 through Apr 30, 2014. Days on which discharge was estimated are marked in orange.

Global cloud datasets indicate that a significant portion of wintertime clouds may be optically thin in the northern hemisphere at mid-latitudes (Rossow and Schiffer, 1999; Stubenrauch et al., 2013; Tselioudis et al., 2013). While thin clouds alter the spectral response of land, in many cases observations performed over thin clouds may still allow identifying land surface features, in particular snow and ice (Riggs and Hall, 2002). This potential is largely neglected in the MODIS snow product generation algorithm where no differentiation between optically thin and thick clouds is made. Developing an ice mapping algorithm which is tolerant of optically thin clouds may substantially improve river ice monitoring.

The focus of this work was on the development of an automated algorithm that generates frequent and accurate river ice maps. The major enhancement is derived from a special treatment of cloudy grid cells. MODIS band 7 (2.1 μm) observations are primarily used to identify clouds, and otherwise to infer information on river ice both from clear sky scenes and scenes affected by semitransparent clouds. The STC algorithm also separates ice detection into three confidence tiers that depend on the observed grid cell reflectance in bands 4 (0.55 μm) and 7. STC also produces several ancillary outputs, including ice fraction and amount time series. False color maps are provided to facilitate visual image interpretation, and to identify flooding. The algorithm was tested and applied over the southern portion of the Lower Susquehanna River basin.

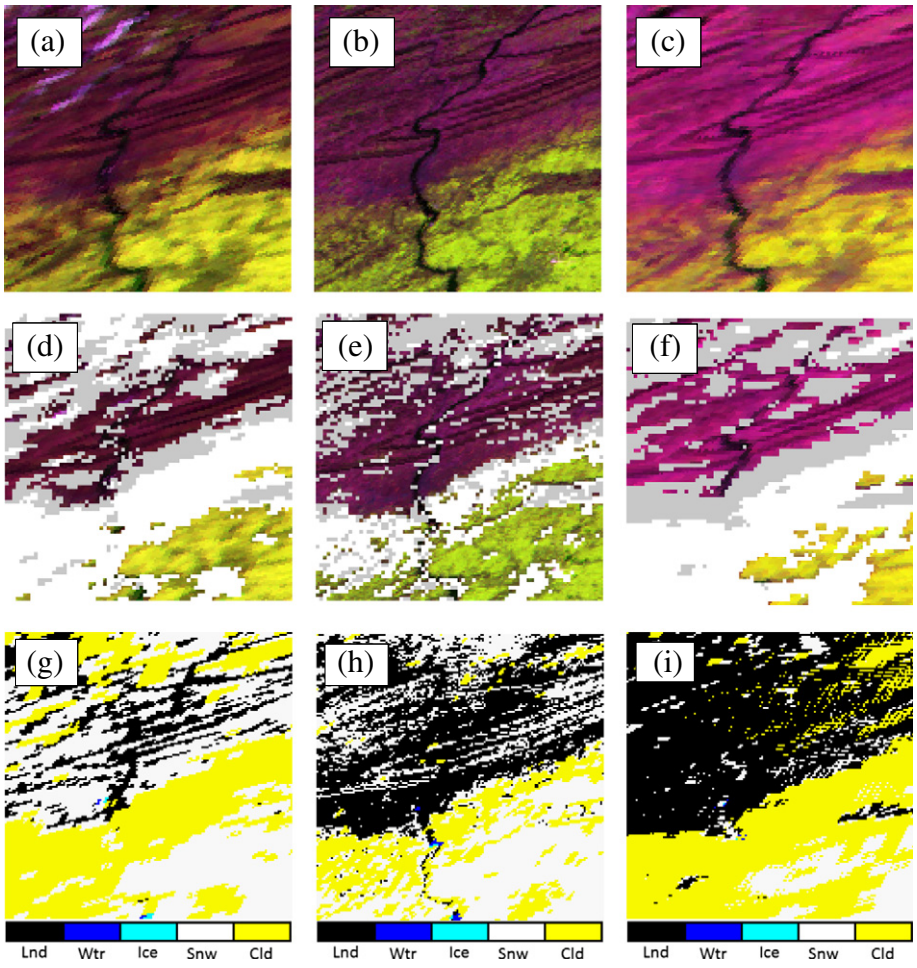

Fig. 3. (a)–(c) Scaled false color images (bands 5, 4, and 7) of study area with (d)–(f) Aqua's cloud information (from MOD35) superimposed (white: cloud, gray: mixed), (g)–(i) MODIS snow product (MYD10A1). The images are for three successive days in 2013 (345, 346 and 347). The snow region is consistently masked as cloudy, and most river grid cells in-between snow cover are also flagged as cloudy.

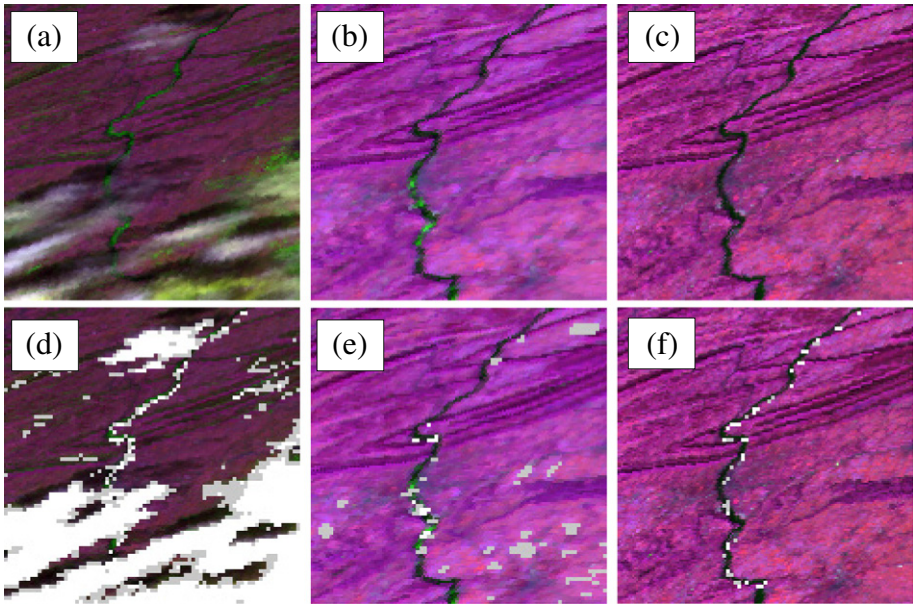

Fig. 4. (a)–(c) Scaled false color images (bands 5, 4, and 7) of study area (2014-070, 2014-016 and 2013-362, respectively) with (d)–(f) Aqua's cloud flag superimposed (white: cloud, gray: mixed). Examples of (a, b) ice-bearing and (c) ice-free river classified as cloudy, in conditions that appear to be clear-sky at these locations. It is notable how well the cloud flag tracks river ice.

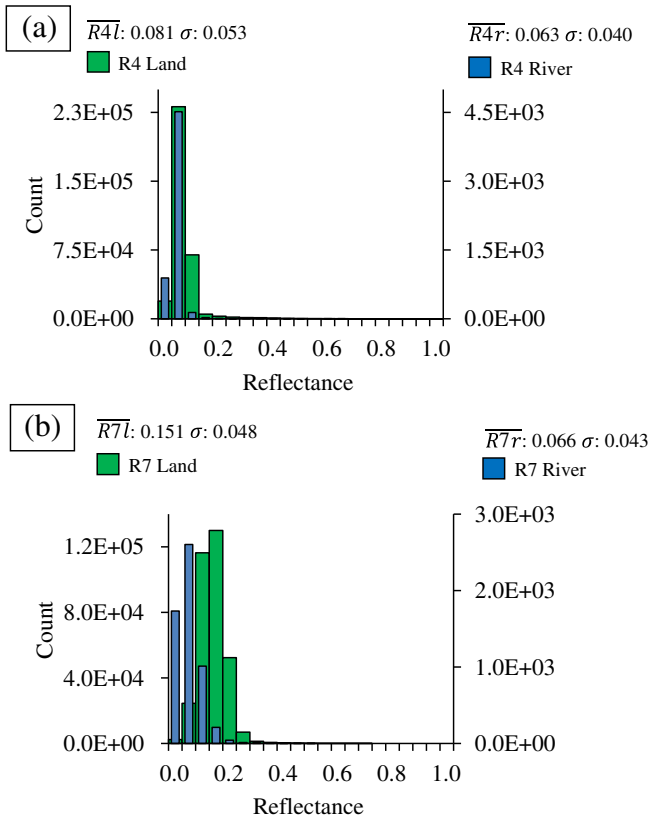

Fig. 5. Histograms for 14 mostly cloud-free 2013-14 winter images. (a) Band 4 for river grid cells and land, (b) band 7 for river grid cells and land.

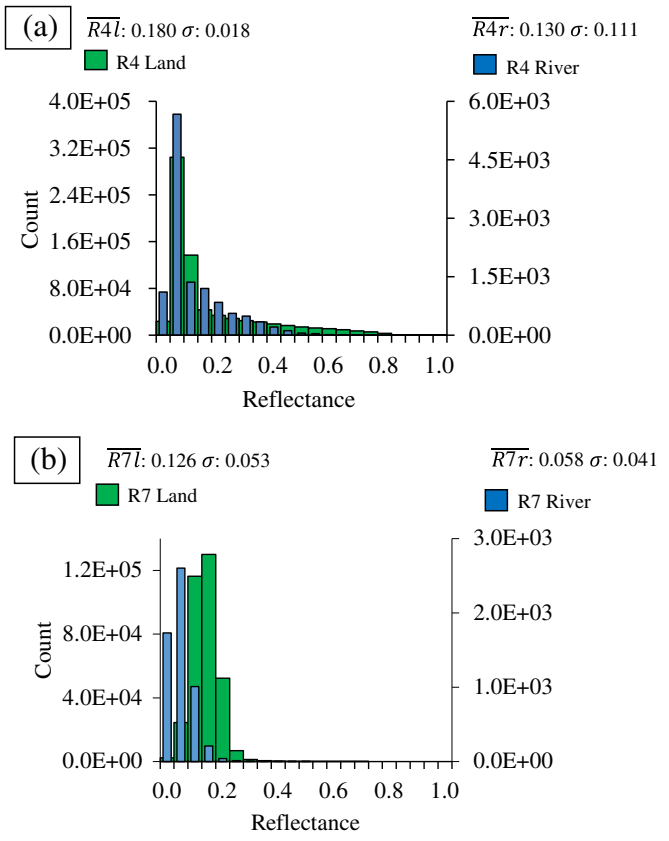

Fig. 6. Histograms of thirty winter images, consisting of those used to produce this figure and an additional 16 thin-cloud images. (a) Band 4 for river grid cells and land, (b) band 7 for river grid cells and land.

2. Study area

The Susquehanna River is a major river in the northeastern United States. It accounts for over 40% of the freshwater flowing into Chesapeake Bay. The river spans six basins for a drainage area of 71,000 km^2, and its main branch is 710 km long and about 1.6 km wide at Harrisburg, PA (SRBC, 2015) (Fig. 1). The Susquehanna basins are considered to be amongst the most flood-prone in the nation. The basins average a severe flood event every 14 years, resulting in a mean annual cost on the order of tens of millions of dollars (SRBC, 2015). Ice jams occur in many parts of the river are of particular concern since they may produce significant flooding when coinciding with high discharge (Fig. 2).

The study region is located in the lower portion of the main branch of the Susquehanna River (Fig. 1a) and covers an area of 70 km^2. The location was selected for its frequent jam occurrence, as taken from the Cold Regions Research and Engineering Laboratory Ice Jam Database (CRREL IJDB), and up to 1.6 km wide river channel, which allows for satellite monitoring at 500 m spatial resolution. For the time period from 2000 to 2012 there were 13 jam related events listed in the IJDB.

3. Datasets and processing

Images were classified based on the MODIS Aqua reflectance product MYD09GA, which includes atmospheric corrections. Data from two spectral bands were used, band 4 centered at 555 nm, and band 7 centered at 2130 nm, along with observation geometry provided within the same product (Vermote et al., 2011). The product is produced on sinusoidal projection with grid cell size of about 0.5 km. Information on the cloud cover within the MODIS scene was obtained from the cloud flag (STATE_QA bit 0–1) also provided in the product. The cloud flag was resampled by replication from 1 km to 500 m spatial resolution. Data for 2014 was utilized for in-depth evaluation of the product, selected due to it being one of the longest and coldest winters at the site since Aqua launched. Two additional winter seasons were processed (2002 and 2003) to make visual comparisons with CRIOS data, available from 2002 to 2012.

The river mask was constructed via supervised classification of three low view zenith angle (VZA) clear sky summer scenes from 2009. The summer time period was selected for the high spectral contrast in the imagery between the land surface and water. Images were classified with a maximum likelihood approach using bands 1–5 and 7 of the MYD09GA product as inputs, corresponding to wavelengths of 0.65, 0.85, 0.47, 0.55, 1.24 and 2.1 μm. The process was repeated for each scene and only grid cells that were classified as open water in all three cases were labeled as river. This conservative approach was applied to exclude mixed grid cells and limit the river mask to open water pixels only. The resulting river mask includes 402 grid cells whereas the entire study area incorporates 24,332 grid cells of the MODIS sinusoidal grid.

Output ice maps are compared against CRIOS ice maps. CRIOS is an automated algorithm that uses MODIS-Terra data as input to produces river ice maps at 0.25 km grid size (Chaouch et al., 2012). CRIOS covers all of the Susquehanna River. It uses MODIS reflectance in band 1 (R1), centered at 650 nm, and in band 2 (R2) centered at 860 nm to discriminate between land and water, water, ice and water and ice. Cloud flags are obtained from MOD09GA. Ice maps are available for 2003–2012.

As an additional source for validation of the output ice maps Landsat 8 imagery was used, obtained from the United States Geological Survey (USGS) via the Global Visualization Viewer (GloVis). Images where the entire river was obscured by clouds were omitted. Only two cloud-free Landsat8 observations occurred at the same day of MODIS observations.

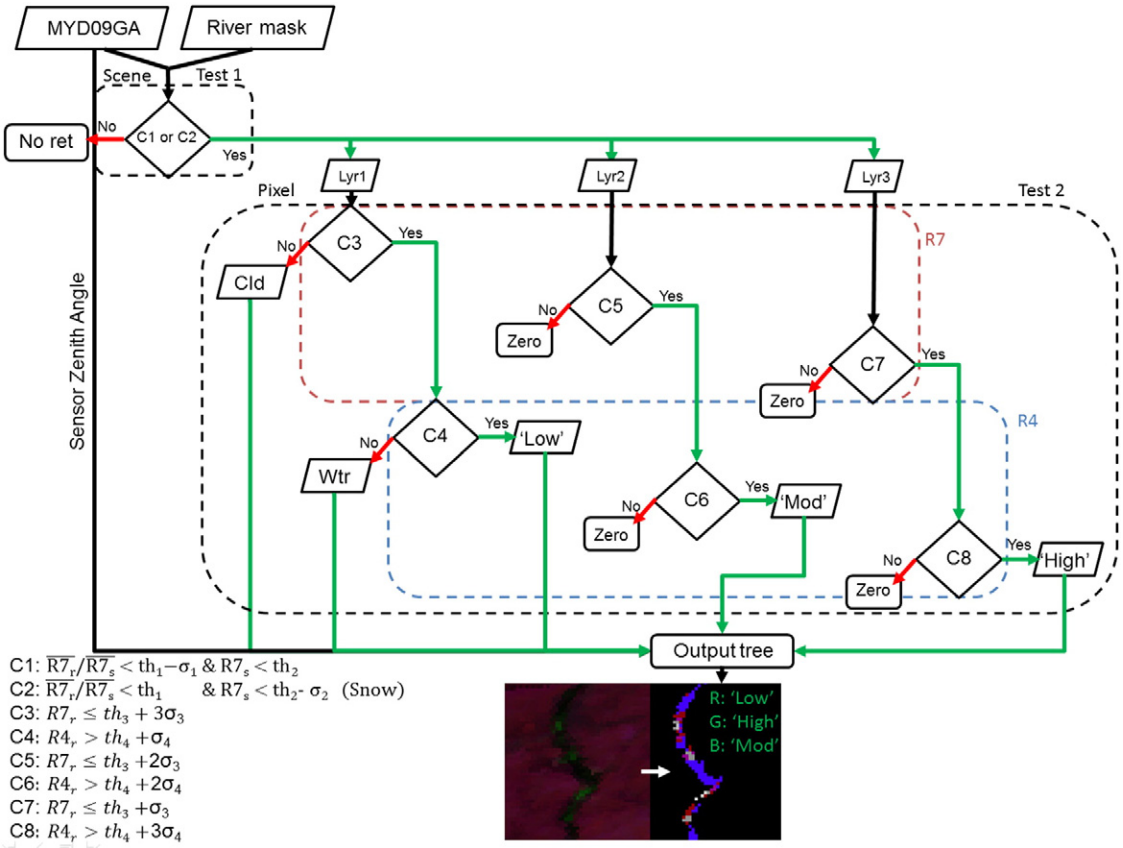

Fig. 7. Flow chart of the STC algorithm used to separate out scenes that are sufficiently cloud-free to proceed working on (C1, C2), and then applies criteria listed in Table 1 (C3–C8) to individual grid cells for ice classification.

Several auxiliary data were also used to facilitate the algorithm development and validation. This includes discharge data and their quality flags for the stream flow gauge at Harrisburg (USGS 01570500), in situ air temperature along with ice jam and flood observation data acquired from the CRREL IJDB (White and Eames, 1999).

4. Physical basis

The goal of this work is to present an ice detection algorithm rather than a detailed analysis of various platforms and their cloud masks. However, as the cloud flag is supposed to highlight locations where data probably should not be used, some discussion is dedicated to the cloud mask's shortcomings and how they relate to river ice monitoring. We show why an approach that forgoes the provided cloud masking is needed at this site: MODIS cloud and snow products are inadequate for river ice monitoring at this site and season. As noted in Section 1, the MODIS cloud mask appears to have frequent false cloud detections at or near locations with snow cover, river ice and land cover transitions.

We present the physical basis and concepts used to distinguish between water, ice, land, snow-covered land and clouds. Histograms based on the 171 wintertime images are generated to establish threshold ranges and frame the algorithm logic. Statistics are generated based on observations in MODIS bands 4 and 7, for river and land. A time series of observed reflectance in band 7 is developed to establish threshold criteria used for the gross cloud screening.

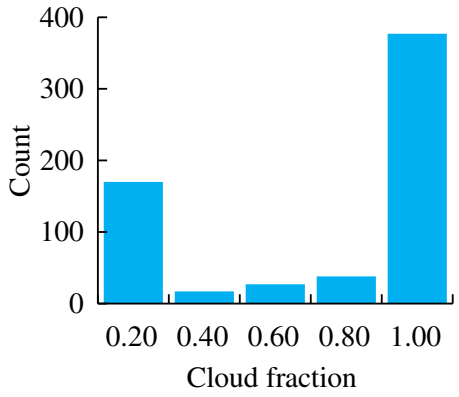

Fig. 8. Cloud fraction quintiles of river grid cells, based on MODIS Terra cloud mask, January–March 2003 to 2012.

4.1. MODIS cloud mask

Cloudiness can often be assessed reasonably well by using the MODIS cloud mask product, but the accuracy of the cloud mask may be greatly impacted by surface and land conditions. The MODIS cloud product is designed to give conservative estimates of cloudiness, meaning that it is biased towards identifying grid cells as cloudy. Unfortunately, adverse conditions exist more often during wintertime, producing frequent cloud cover overestimation at the study region.

Fig. 3 is represented in false colors with MODIS bands 5, 4 and 7 mapped to red, green and blue, respectively. In a band 5, 4, and 7 false color display water, ice, land, snow and clouds appear approximately black, green, red, yellow and white, respectively. In most cases, snow cover appears to cause false cloud detections which usually cause the river grid cells in-between snow cover to be flagged as cloudy (Fig. 3). Part of the reason may have to do with the mask being 1 km resolution, thus allowing the possibility that it extends one or more grid cells into the river if depending on viewing geometry. While cloud mask differences may exist between Figs. 3 and 4 (explained in Riggs and Hall, 2004), both indicate a significant portion of apparent snow cover

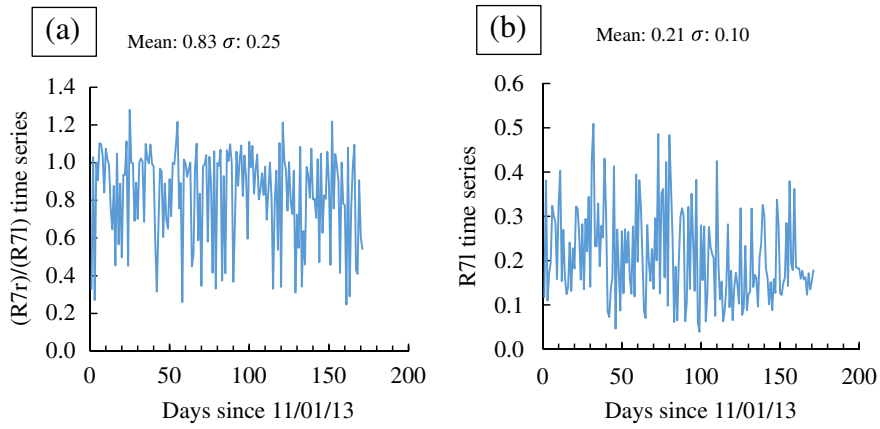

Fig. 9. a) Time series of $\overline{R7r}/\overline{R7l}$. Low ratios indicate that the river is separable from land and the scene has limited or no cloud coverage. b) Time series of $\overline{R7l}$.

classified as cloud. The blurriness in Fig. 4a and c is due to observations performed at large VZA (57°). Classifications performed at large VZA are more challenging and the quality of the cloud mask is also impacted (Maddux et al., 2010). Even at small VZA values (i.e. 2°, Fig. 4b), snow covered adjacent grid cells increase the reflectance at river grid cells and may result in misclassified ice if thresholds are set too low.

Additional shortcomings of the snow product for use in river ice monitoring include that most of the cloud-free river grid cells are masked as land (Fig. 3g and h), the occurrence of false ice detections, and the cloud-free river being misclassified as snow covered (Fig. 3i) although it is apparently free of snow and ice. Evidently, the collection 5 snow product (the fifth reprocessing of MODIS products) is not reliable for this investigation.

Accurate cloud identification is further complicated at locations that may experience significant spectral variation over time, as is the case with rivers transitioning between open water and ice cover. In case of MODIS Aqua, we observed several instances of river ice classified as cloud, although there were no apparent clouds in the vicinity (Fig. 4).

The shortcomings of the cloud mask aggregate to eliminate a large amount of reasonable data points, especially with regards to river ice. In order to produce frequent ice maps, an alternative approach is needed.

4.2. Establishing thresholds for land, water, ice, snow and clouds

Ice, similar to snow, has high reflectance in the visible and low reflectance in the shortwave infrared. Therefore primary MODIS reflectance bands for ice detection are those similarly used in snow detection: one visible band (band 4) and one shortwave infrared band (SWIR), here band 7. The SWIR reflective spectral band is needed to discriminate clouds from snow. It is well established that water, snow and ice are readily identified based on their spectral properties in the visible and the SWIR (Hall et al., 2002; Satterwhite et al., 2003; Warren, 1982). Depending on land cover type, SWIR bands such as MODIS bands 6 and 7 may also be used to discriminate between land and snow, since snow cover strongly masks the underlying surface (Satterwhite et al., 2003). These bands are helpful for observing river grid cells because other than for cloud cover, river grid points can be expected to have near zero reflectance in the SWIR, irrespective of if they contain ice, open water or snow. MODIS band 5 is used to supplement false color images, to highlight locations of snow cover and clouds more clearly. Since reflectance values at any grid point are partially influenced by adjacent land grid cells it is important to know whether the land surface near the river is snow covered.

This section examines the spectral properties of land and river scenes, and shows how thresholds to be used to discriminate between water, ice, land, snow and clouds in the MODIS image are derived. For reference, 'scene' is used to refer to the entire field of view, while 'land' is used to describe portions of the scene that are not part of the river mask. For this study the 2014 winter season was examined, consisting of 171 daily images covering the time period from November 1, 2013 to April 20, 2014. Thirty high quality images characterized by low VZA were selected for analysis. Fourteen images (referred here and below as set 1) represented the situation with no snow cover on land, no ice cover on water and <10% cloud cover over the river as per the cloud mask product. In the remaining sixteen images (set 2) the river bore ice and land was mostly snow-covered.

Figs. 5 and 6 present the frequency histograms of the reflectance in bands 4 and 7 over the land surface and over the river obtained from the first set of images (Fig. 5) and from the first and second sets combined (Fig. 6). Their characteristics are in line with the physical basis described above, and are indicative of ice cover rather than cloud. Over the river, reflectance in band 4 incorporating both sets of images was larger than if only ice-free observations were included (set 1) (Fig. 6a). At the same time the reflectance in band 7 over river ($\overline{R7r}$) in both sets remained nearly identical (Figs. 5b and 6b). The tail over the river in Fig. 6a is mainly due to some of the river grid cells having higher reflectance than others, since image selection was done carefully and scenes with optically thick clouds were avoided. We mainly attribute the tail being due a range of ice concentration within the river grid cells. The tail also suggests that it may be valuable to develop thresholds between a completely ice-free and ice covered state. Band 4 reflectance for land also has a tail (Fig. 6a), and is mainly due to snow. As it follows from Figs. 5b and 6d the mean reflectance of the snow covered land in band 7 ($\overline{R7l}$) is 17% lower than the reflectance of the snow-free land surface. The observed smaller mean reflectance in MODIS band 7 for snow-covered land is consistent with the fact that the spectral reflectance of snow in the shortwave infrared spectral range is generally smaller than the reflectance of the snow-free land surface.

Many of the sixteen images in set 2 were flagged as mostly cloudy by the MODIS cloud mask. Yet a lower rather than higher mean reflectance is observed in band 7 over land. This suggests that clouds (if any) are too thin to have a significant impact, as band 7 reflectance is expected to increase if clouds are present (with respect to bare land or snow at this site). We conclude that the reflectance decrease is mainly attributable to the change of the land surface cover properties; specifically the masking by snow. The overall 17% reflectance decrease is significant, considering that several of the sixteen additional images only exhibit partial snow cover, and also include snow-free scenes. This suggests that band 7 reflectance can be used to roughly characterize whether the field of view consists of bare land, snow covered land, or clouds. This observation is relevant for the algorithm's coarse scene classification, referred to as test 1, explained in Section 5.1.

We roughly estimate the confidence of a grid cell being correctly classified as ice using band 4 and band 7 tests, with thresholds based

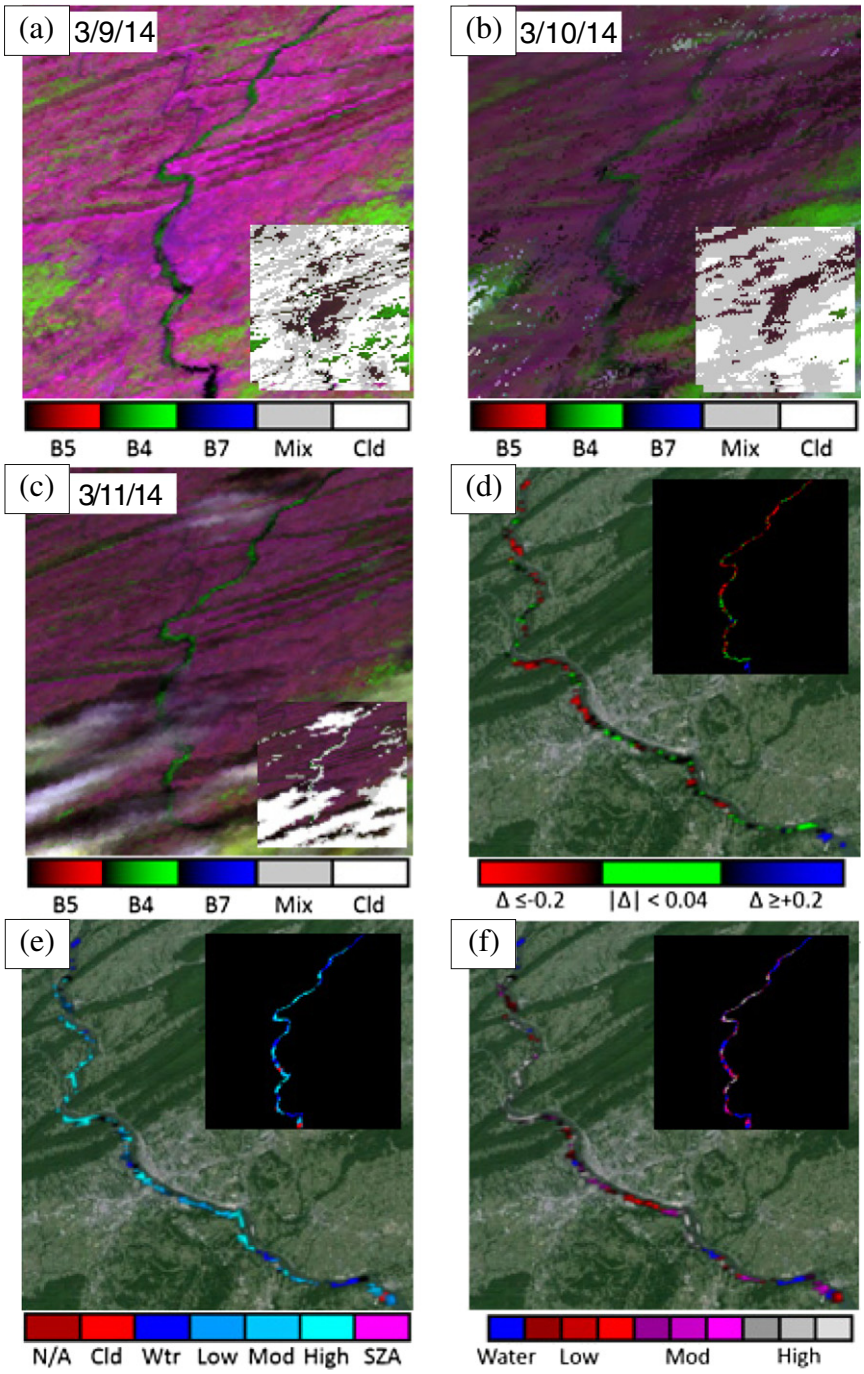

Fig. 10. (a)–(c) Full scene scaled false color with insets showing cloud flag (white: cloud, gray: mixed). (d)–(f) Algorithm outputs projected for display on Google Earth with insets of corresponding outputs on sinusoidal grid: d) reflectance change, e) ice confidence, f) running composite ice map colored according to confidence and reflectance magnitude.

on Fig. 5 histograms. Limits are imposed such that the low confidence range has the most generous classification for what could be ice, while moderate and high ice have to meet stricter criteria (Table 1). In this scheme, grid cells that have high band 4 and low band 7 reflectance have higher confidence of being ice. The scheme presented in Table 1 represents a starting point and may be revisited to improve ice classification. For example, if the algorithm overestimates river ice due to adjacent snow cover, band 4 thresholds may be increased. Likewise, band 7 thresholds for clouds may be decreased below that indicated in the table to reduce the likelihood of clouds being identified as ice.

In conclusion, the ice detection algorithm is not based on a single binary test, since varying ice concentrations and cloud optical thickness span a range of reflectance. Instead, due to the chance of more or less thin clouds being present in any one grid cell, ice will be classified within confidence ranges. Also, band 7 is found to be effective at discriminating between land, snow covered land, and clouds at this site and it will be used in a gross classification scheme of the scene being investigated, test 1. The significance of test 1 will be addressed in Section 5.1.

5. Algorithm

Overall, the STC algorithm consists of three major stages. Stage 1 is referred to as test 1, and is the preliminary cloud and snow test, to determine whether the scene is relatively free of clouds, snow is present,

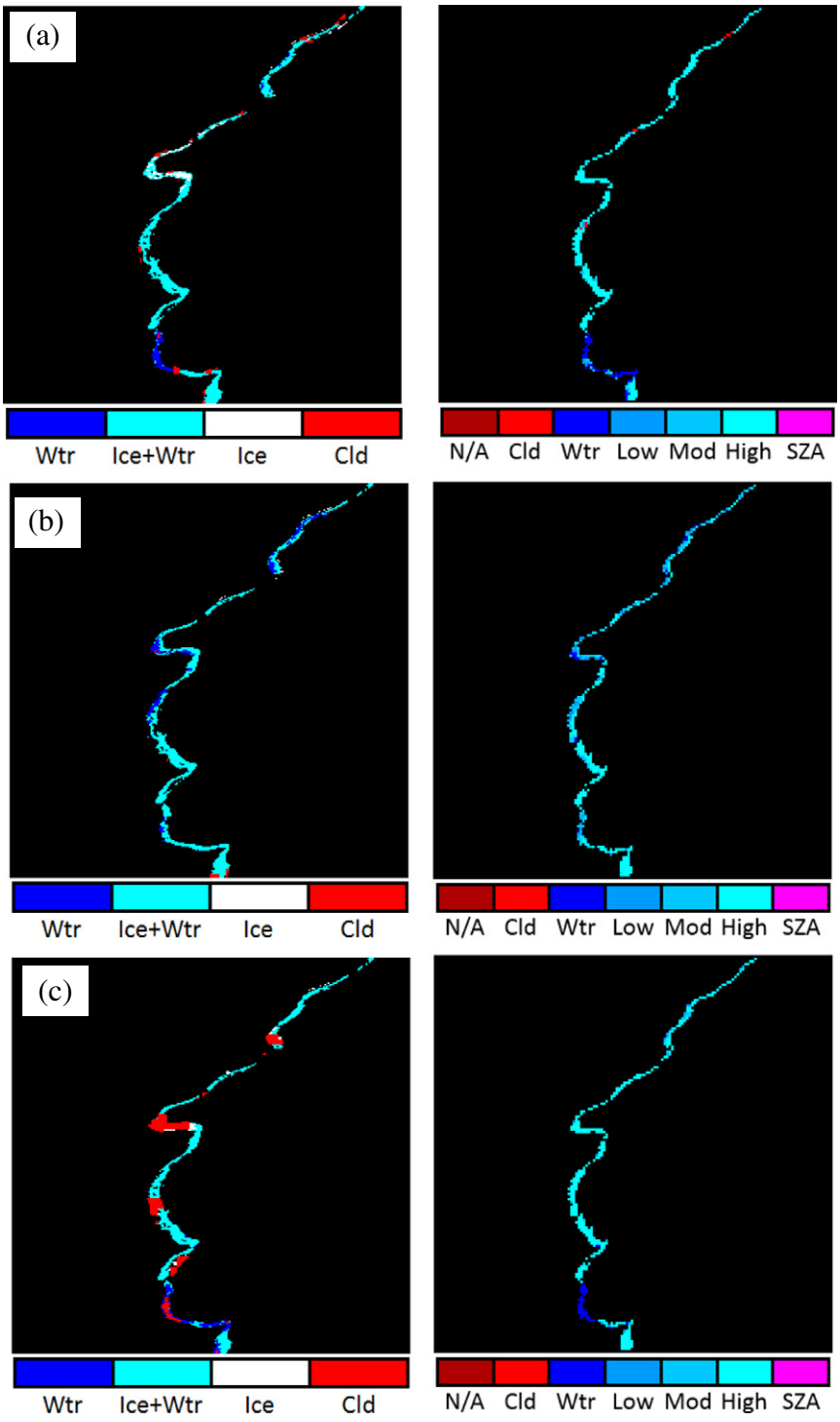

Fig. 11. Left: CRIOS (Terra) ice maps, using global cloud mask; right: Algorithm ice maps with local cloud mask for days (a) 2003-24, (b) 2004-016 and (c) 2004-050.

or is too cloudy to process further. Test 1 consists of two conditions, at least one of which needs to be met to proceed: 1) low cloud cover over bare land and/or 2) low cloud cover over snow-covered land. If the scene passes test 1, all grid cells falling within the river channel are passed to stage 2, where river grid cells are subjected to a further pixel-by-pixel classification, test 2 (Table 1). Within this classification thick clouds are identified first, which are those that fail to meet condition C3. The remaining river grid cells are classified into open water and three confidence levels of ice detection. Stage 3 is loosely termed the output tree, which performs data operations and generates additional outputs (i.e. maps for ice cover duration, reflectance change).

5.1. Test 1: preliminary cloud & snow identification

A first estimate of cloud cover within the scene is based on the spectral contrast provided between land and river grid cells evaluated from the ratio of their respective mean reflectance. The idea is that in a cloud covered scene of limited spatial extent (allowing for assumption of uniform cloud cover), the mean reflectance of river grid cells would resemble that of land grid cells with a ratio near unity. In scenes where river grids are predominantly cloud-free, land and river grid cells are expected to feature distinct reflectance (C1). As snow covered land resembles the reflectance of cloud-free river, an alternate thresholding condition

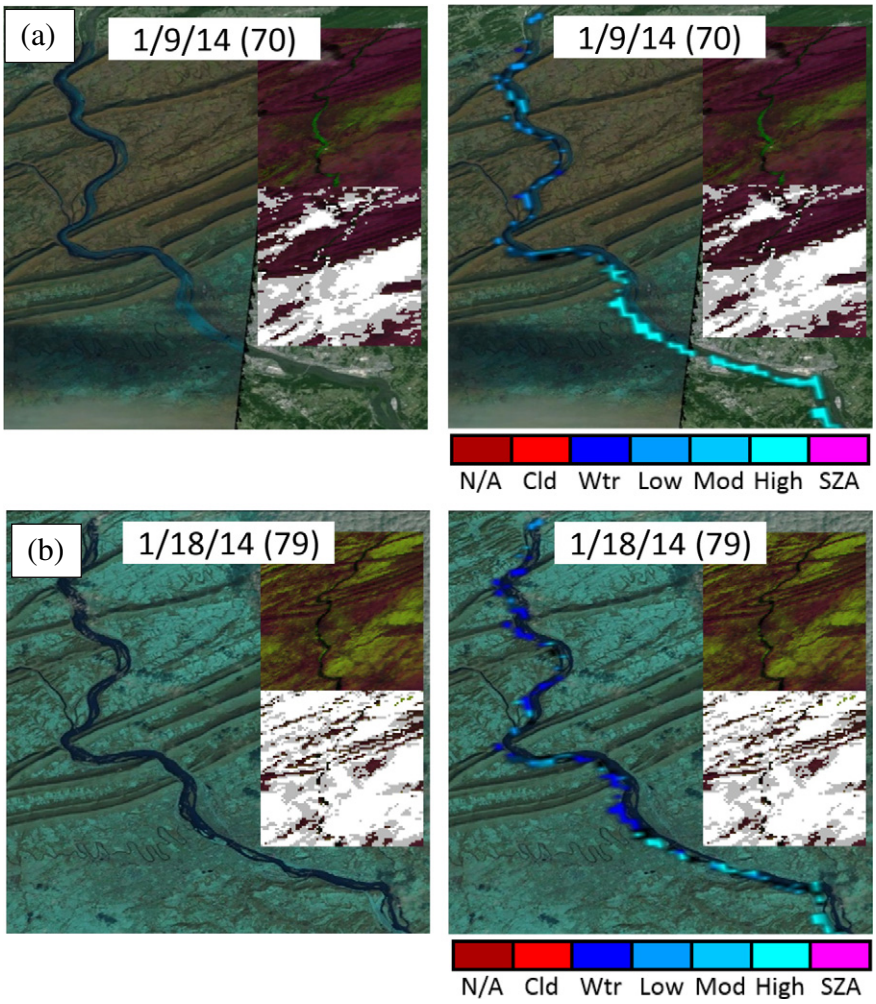

Fig. 12. Comparison of Landsat 8 imagery (left) with ice maps derived from STC overlaid on top of Landsat 8 imagery (right), and insets of Aqua false color images and corresponding cloud mask.

(C2) is implemented. Means and standard deviations of the land/water contrast time series are used to determine delineating thresholds. Conditions C3 through C8 represent test 2 and are used to establish ice confidence levels as described in Table 1.

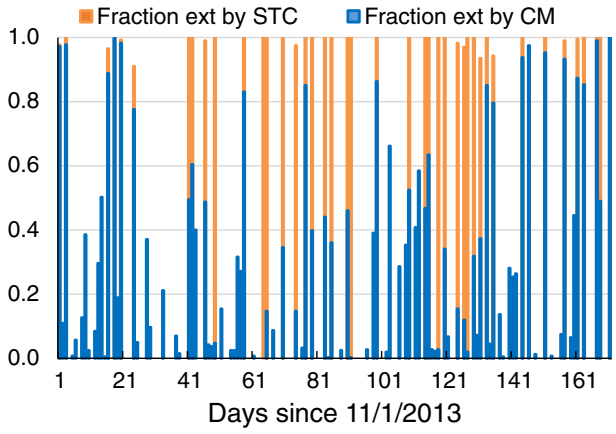

Fig. 13. Time series of the fraction of river grid cells available for ice retrievals as determined from the MODIS cloud mask (blue) and with STC (orange).

We use band 7 averages over the land and river to assess the presence of cloud and snow within the scene. Based on 10 years of winter data (2003 − 2012), cloud cover over river in the first and fifth quintile account for 86% of the all cases (Fig. 8). We use this data infer that cloud coverage may be assumed mostly uniformly distributed within the study region (fully cloudy or fully clear) and time period. Thus, band 7 reflectance values averaged for land grid cells should be able to assess whether individual scenes are cloudy at this limited spatial scale.

Preliminary cloud identification consists of the ratio of the mean reflectance of the river grid cells ($\overline{R7r}$, total: 402) to that of the land grid cells ($\overline{R7l}$, total: 23,930). Referring to Fig. 5 histogram, clear river scenes have small values for $\overline{R7r}$ (~0.066), while snow-free land has considerably larger $\overline{R7l}$ reflectance (~0.15), yielding a ratio of 0.43. When cloud covered, the expectation is that this ratio approaches unity.

The daily time series of $\overline{R7r}/\overline{R7l}$ (Fig. 9a), show that 1) there are large day to day variations, 2) that it is not uncommon for reflectance ratios to exceed unity and 3) that the ratio rarely exceeds 1.1, but often may be significantly less than unity. The winter mean value of $\overline{R7r}/\overline{R7l}$ is 0.83, which indicates that river grid cells on average are not readily separated from land, due to cloudy conditions or snow. Larger $\overline{R7r}/\overline{R7l}$ ratios may also occur in the case of snow-covered land, since snow cover masks land and $\overline{R7l}$ may approximate $\overline{R7r}$. To account for the snow-covered scenario, a second threshold condition is implemented. The alternative test is allowed on the basis that when $\overline{R7l}$ is depressed due to snow,

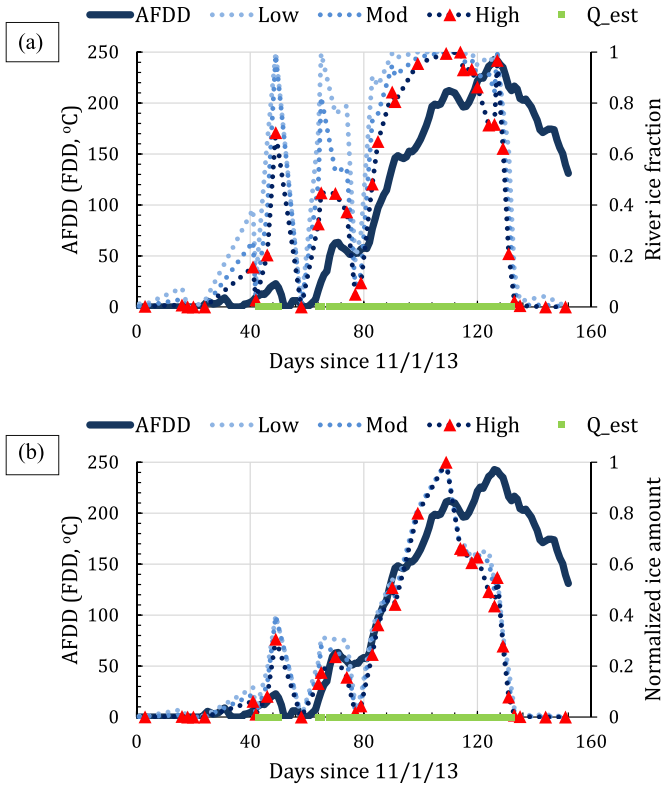

Fig. 14. Time series of (a) the fraction of the 402 grid cells classified as river ice at three confidence levels and (b) the normalized sum of river ice reflectance (ice amount) versus AFDD. Triangles indicate days on which STC sampled the river and Q_est represents days on which ice presence was inferred from the USGS gauge.

enough information from the surface should also be available over the river to determine whether ice is present or not.

For both cases an additional requirement is imposed on the denominator: that the magnitude of $\overline{R7l}$ must also be small. For the snow-free case, $\overline{R7l}$ must be less than the wintertime mean value established in Fig. 9b. When snow cover is present, the $\overline{R7l}$ threshold should be decreased (i.e. by one standard deviation, to 0.11): since snow cover decreases $\overline{R7l}$, too many clouds would be allowed if the same threshold as that of the snow-free case were used. This allowance for snow covered land permits 30% more scenes to be selected for processing. The criteria, shown in Table 2, are informed by the means and standard deviations obtained from the time series shown in Fig. 9.

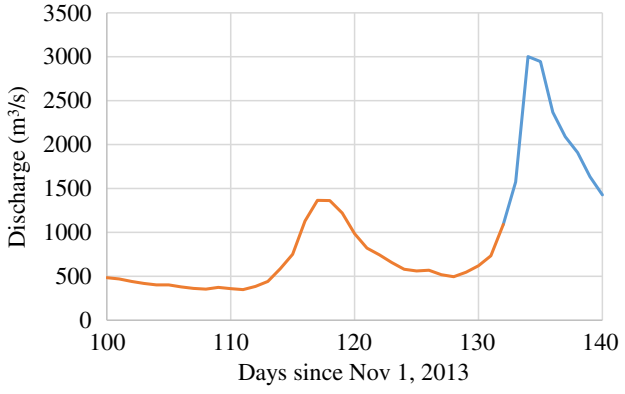

Fig. 15. Daily mean discharge for days 100–140 since Nov 1, 2013. The first discharge peak occurs on day 117, followed by a larger peak on day 134.

While this test is somewhat crude and has its limitations, there were only few instances where snow covered scenes of reasonable quality were not selected for further processing. An example is the case of partial snow cover shown in Fig. 3a ($\overline{R7r}/\overline{R7l}$: 0.59; $\overline{R7l}$: 0.086) and b ($\overline{R7r}/\overline{R7l}$: 0.32; $\overline{R7l}$: 0.073): test1 determined that at least one of C1 and C2 were satisfied, while for the scene shown in Fig. 3c ($\overline{R7r}/\overline{R7l}$: 0.66; $\overline{R7l}$: 0.136) neither criteria was met. Of the three scenes, Fig. 3b is of the highest quality, and as result met both criteria. Both Fig. 3a and c appear blurry due to being located closer to the edge of the scan. Their respective VZA angles are 57 and 58°, and as result have larger $\overline{R7r}/\overline{R7l}$ ratios, indicating that river and the snow covered land are less clearly separated.

A breakdown of relevant statistics for those images passing conditions C1, C2 or both is provided in Table 3. A rough categorization of whether the scene contained snow and ice was done by visual inspection. Results show that the categorization between snow-free and snow scenes is excellent, doing so correctly in 21 out of 22 cases. The exception is day 2013-307 ($\overline{R7r}/\overline{R7l}$: 0.27; $\overline{R7l}$: 0.1098) where $\overline{R7l}$ barely satisfies the threshold of 0.11. Table 3 also shows that VZA tends to be significantly larger for those scenes that only meet either C1 or C2 (>30°) compared to those meeting both criteria (20°). It also illustrates that effort should be taken to screen-in snow covered scenes for processing, since an additional 6 scenes containing ice can be included, increasing the winter total from 11 to 17 scenes.

5.2. Test 2: image classification

Test 2 consists of two steps. In the first step, band 7 reflectance tests are applied to river grid cells, in three layers. The lowest confidence layer is most tolerant of clouds (allowing band 7 values equal up to $\overline{R7r} + 3\sigma$ as per condition C3), and grid cells that fall above the threshold are considered cloudy. For the two higher confidence layers, grid cells that don't meet their respective conditions (C5 and C7) are set to zero. Conditions are applied likewise to the visible band (R4), with the low confidence layer used to delineate between open water and ice. The image classification scheme is presented in more detail in Section 4.2 with criteria and thresholds shown in Table 1.

The algorithm produces several outputs, some of which are shown in Fig. 10. Fig. 10a–c shows false color scenes (bands 5, 4 and 7) for March 9 through 11 (days 129–131). The March 10 image (Fig. 10b) failed test 1 ($\overline{R7r}/\overline{R7l}$: 0.72; $\overline{R7l}$: 0.122), and ice maps are not produced. Cloud mask insets show that the region was mostly cloudy on March 9, mostly mixed and cloudy on March 10, and mostly cloudy and clear-sky on March 11. False color images may also show flood inundation (not observed in 2014).

Fig. 10d–f shows reflectance change (here with respect to Fig. 10a), ice confidence and running composite maps based on the March 11, 2014 scene (Fig. 10c). March 11 is near the end of the ice bearing period, and the river becomes mostly ice-free on March 13. Fig. 10a–c can't be directly used to visually establish the reflectance differences, since they were scaled for display. The reflectance change map is composed of reflectance differences of band 4, between the most current and last observed value at a given cloud-free grid cell. Its purpose is to highlight regions that experience significant reflectance change, which may be interpreted as changes in ice mobility or ice concentration. On March 11, clouds affect a significant part of the river. However, at locations away from thick clouds the reflectance change map can be used to identify the trend in the ice accumulation or dissipation. Fig. 10d shows an overall decrease in reflectance at locations away from clouds and is consistent with ice dissipation in line the above freezing temperatures that persisted starting March 7 (Table 4). The small region of river affected by cloud shadow produces a false water classification (Fig. 10e). Locations, near which thick clouds can be seen, are found to have increased reflectance, falsely resulting in similar (green) or greater values (blue,

Table 1
Concurrent requirements on bands 4 and 7, to classify water, clouds and ice. Low, mod and high refer to the confidence of ice identification. Specific values are obtained from histogram statistics of river grid cells for bands 4 and 7, shown in Fig. 6. These values constitute test 2 of the algorithm (Fig. 7).

Band/class	Low	Mod	High	Cloud	Water
B4	$>\overline{R4r}+\sigma$	$>\overline{R4r}+2\sigma$	$>\overline{R4r}+3\sigma$	NA	$\leq\overline{R4r}+\sigma$
	>0.103	>0.143	>0.183	NA	≤0.103
B7	$\leq\overline{R7r}+3\sigma$	$\leq\overline{R7r}+2\sigma$	$\leq\overline{R7r}+\sigma$	$>\overline{R7r}+3\sigma$	$\leq\overline{R7r}+3\sigma$
	≤0.195	≤0.152	≤0.109	>0.195	≤0.195

south edge) compared to March 9, but are correctly flagged as lower confidence ice in Fig. 10f.

6. Results

6.1. Validation by visual inspection (CRIOS/LANDSAT8)

Ice maps produced by STC are in good agreement with CRIOS (Fig. 11). It is notable that CRIOS often indicates cloud cover near the riverbanks, potentially due to false cloud detections within the global cloud product. Otherwise, ice maps are in good agreement, although STC was set-up based on 2014 statistics and then applied to imagery from 2003 and 2004.

Fig. 12 shows MODIS Aqua based ice maps compared to available Landsat8 imagery for available occasions (same day, river visible) for 2014. While comparisons are made on the same day, there may be differences due to overpass timing. Fig. 12a and b show that the algorithm is sensitive to small amounts of ice. Fig. 12b has several instances of border ice that are correctly classified, predominantly in the lower third of the image. False detection may be attributed to snow cover at riverbanks and islands impacting the reflectance in adjacent grid cells. In this study, the threshold for river ice detection is small, and false ice classification may occur frequently. This may be addressed by increasing the threshold used to delineate river ice.

6.2. River observations: cloud mask

Fig. 13 demonstrates that replacing the MODIS global cloud mask with the cloud screening approach of STC algorithm results in a significant improvement in data availability. Fig. 13 compares the fraction of river grid cells, out of 402, identified as cloud-free by the MODIS cloud mask and by STC. The improvement, referenced to days elapsed since Nov 1, 2013, is mostly seen during the Dec 13, 2013 (day 43) to Mar 12, 2014 (day 132) time period when the river and land were for the most part ice and snow-covered. Application of the MODIS standard cloud mask (CM) often results in few cloud-free grid cells on a given day. Between days 43 and 132, there were only seven occasions on which >50% of the river was identified as cloud-free by the CM. Lack of data during this period is of particular concern, since the river bore ice only during these 90 days. Ice bearing dates were established from daily USGS discharge quality data flags, explained in Section 6.3.

The effective revisit time using the CM was slightly better than for the STC algorithm when the river was ice-free (Table 5). While the river bore ice, using the CM nearly doubled the effective revisit time (7.1 days). Since both approaches have close to identical revisit times otherwise, the differences are most likely explained by cloud mask errors with respect to snow and ice rather than significant change in cloud cover. Using STC, the effective revisit time does not vary greatly regardless of whether the river or land bear ice or snow.

Using the CM, 8 out of the first 42 days (matching ALG 100%) and 10 out of the last 39 days (matching ALG 90%; CM indicates 49% cloud free on day 168) show >50% of river grid cells as clear sky. However during the intermediate 90 day period, there are only seven occasions where the MODIS cloud mask maps 50% or more of the river as not cloudy. However, STC considers 24 days not particularly cloudy during this time.

The CM approach only yields about 402 grid points more data over each 40-day open-water time period (ΔData ~ 1.0). It does so over many more days, 25 vs 8 and 22 vs 10 for CM vs STC, respectively. STC does not frequently classify grid cells as cloudy, as evidenced by the data amount closely approximating the amount of observation days (23.9 vs 24 days). This suggests that the 'low' probability threshold may be too generous to clouds and/or that cloud cover of the scenes passing test 1 tend to consist of semitransparent, uniformly distributed clouds. The overall effective revisit times for 2014 are 5.2 vs 4.1 days (computed from 171/ΣData), sampled from 95 vs 42 days for CM vs STC, respectively.

Table 3
Breakdown of scenes that pass coarse cloud-screening, test 1.

Criteria	# scenes	AVG VZA	# snow scenes	# river ice scenes
C1 only	20	33.6	0	4
C2 only	9	40.6	9	6
C1 & C2	13	19.1	12	7
Totals	42	30.2	21	17

6.3. Consistency of ice maps with ancillary data

Ancillary information can be used to evaluate the performance of the algorithm. Ancillary data consists of the air temperature record, ice related reports in the IJDB and USGS discharge estimates. These ancillary datasets are important since they provide credible information on ice processes on the river, against which ice maps may be validated. The daily USGS data flag for an occurrence of a discharge estimate is used to qualitatively determine that river ice was present on a given day. The in situ air temperature record is important as it can be related to ice growth and dissipation. Ice jam warnings and observations entered in the IJDB are useful for obtaining the timing and duration of ice jams, and also allows inference of whether river ice was present.

Fig. 14 compares the low, mod and high ice confidence levels with the USGS time periods of discharge estimates and accumulated freezing day degrees (AFDD). AFDD is relevant for empirical ice growth modeling (Stefan, 1891) and is frequently used due to its simple form and generally good results (Zubov, 1963). Fig. 14a shows the time series of river ice extent, represented by the portion of the 402 river grid cells classified as ice. Fig. 14b shows the time series of river ice amount. River ice amount is calculated by summing the band 4 reflectances of river grid cells classified as ice, and then normalizing with respect to its winter maximum.

River ice amount provides helpful context for assessing gird cells classified as ice bearing. It roughly informs on by how much the thresholds for ice classifications are exceeded, on average. For example, although Fig. 14a shows that a large portion of the 402 grid cells may be classified as ice covered (68%–100%) on day 49 (Dec 19, 2013), Fig. 14b for the same day shows a net reflectance which is significantly

Table 2
Criteria for coarse cloud-screening.

Criteria	Condition	Outcome (if criteria met)
C1	$\overline{R7r}/\overline{R7l}<0.58; \overline{R7l}<0.21$	Bare land, pass
C2	$\overline{R7r}/\overline{R7l}<0.83; \overline{R7l}<0.11$	Snow, pass

Table 4
Temperatures March 7, 2014 through 11, 2014, at Middletown PA.

Date	3/6	3/7	3/8	3/9	3/10	3/11
T (°C)	−4	1	4	3	9	10

Table 5
Comparison of the MODIS cloud mask and the algorithm cloud mask. Data: number of river observations, computed by summing the ratio of observable grid cells divided by the total (402), Obs: number of days in which at least one grid cell was observed, Rev: effective revisit time (days).

Days since 11/01/13	MODIS cloud mask			Algorithm		
	Data	Obs (days)	Rev (days)	Data	Obs (days)	Rev (days)
1–42 (42 days, no ice)	9.3	25	4.5	7.8	8	5.4
43–132 (90 days, ice)	12.7	48	7.1	23.9	24	3.8
133–171 (39 days, no ice)	11.2	22	3.5	9.9	10	3.9

lower than the wintertime maximum. The low net reflectance suggests that ice classification occurred with low threshold exceedance and predominantly low ice concentrations prevail. The USGS issued discharge estimates between days 43 through 50, suggesting that some ice was present within the field of view. This is corroborated by the ice time series generated from the satellite data which also supports that river ice disappeared between days 49 to 58. The peak value of AFDD is small (19 FDD), which suggests a limited amount of ice which is more likely to flow without causing ice jams. The CRREL IJDB didn't show a jam related entry at this time. A second cold wave, peaking on day 71 (Jan 10, 2014), may be assessed similarly. Here, the AFDD peak value is considerably larger (63 FDD), suggesting more ice. Although ice amount and ice extent are lower than those of day 49, the satellite image indicates a significant concentration of ice in the mid portion of the field of view (Fig. 3). The CRREL IJDB states that this ice accumulation was an ice jam starting Jan 8 which remained in place until about Jan 14. The day 49 ice maps are likely to be ice overestimates, due to clouds and/or viewing geometry. Days on which overestimates occur may be inferred from large differences between ice confidence levels.

The AFDD curve is constructed from air temperature measurements located at Middletown, PA, available from Weather Underground (Fig. 14). A positive slope represents cooling, and its magnitude indicates the rate. Ice extent and ice amount follow the AFDD curve fairly closely. The AFDD indicates warming from days 109 through 114 (negative slope), and satellite observations (days 109 and 114) indicate a large decrease with respect to ice amount (Fig. 14b) rather than ice fraction. The decrease in ice amount can be explained in context with increased discharge, which can lower ice concentration. Fig. 15 shows that discharge between days 109 and 114 increased by nearly 60%, eventually peaking at 1360 m^3/s on days 117/118. In general, discharge magnitude estimates by USGS support the observed ice processes, in that low flows are conducive ice formation and increased flows can break-up and dilute ice.

Days of significant ice presence are inferred from the discharge data quality flag. USGS reverts to discharge estimates starting on day 43 (Dec 13, 2013) and ending on day 133 (Mar 12, 2014). This time range also has two thaw periods; periods of successive days during which USGS indicates discharge observations as opposed to estimates (Figs. 2, 14 and 15). The rationale for using the USGS data quality flag to infer ice presence is based on the hydraulics of frozen or ice-bearing rivers being different from their open channel equivalents introducing errors. Days on which discharge errors are estimated to be large are flagged estimates. For purposes of validation, we assume river ice to be present wherever estimates replace the measured values. Comparing the USGS discharge flags with STC ice maps shows that there are no non-detections. We suspect one instance of false alarm occurring on day 41 (high: 16%, low: 38%) due to the subsequent observation on day 42 (Fig. 3b) indicating nearly zero ice extent. This is likely due to the day 41 observation having occurred near the edge of the scan, and the snow adjacent to the riverbank producing several false ice detections. The observation on day 42 occurred at nadir, and is more credible. We suspect other potential ice overestimations due to adjacent snow cover (i.e. day 65). However, this is difficult to verify as low ice concentrations and border ice may also result in a grid cell classified as ice. As observing low ice concentrations may not be relevant, ice detection thresholds for band 4 can be further increased beyond those shown in Table 1 to reduce false detections. False ice detections are found to be primarily due to processing of scenes that have large VZA where riverbanks are snow covered, rather than due misclassifications of clouds as ice.

According to the CRREL IJDB, ice jams occurred at: 1) Middletown on day 69 (Jan 8), 2) Marietta on day 84 (Jan 23) and 3) at Harrisburg (City Island) until at least day 103 (Feb 11). Harrisburg and Middletown are located near the center of the field of view, while Marietta is located adjacent to the river at the south edge. The ice jam first observed on day 69 was clearly visible on day 70 (Fig. 3). Jam related flood watches or warnings were issued for days 69, 70 and 75 at Middletown. The algorithm's ice outputs shown in Fig. 15 are consistent with these entries as the algorithm observed significant river ice on or near each of these dates.

7. Conclusions

We find that an algorithm that first checks the scene for clouds, and second operates on grid points individually to classify between water, ice and clouds presents a good alternative to using the Aqua cloud product. Although the STC algorithm produces some misclassifications, it is reliable and produces more frequent opportunities to observe river ice. Occasional misclassifications may occur at the edges of clouds, cloud shadows and adjacent to snow covered riverbanks. The algorithm is shown to be sensitive to river ice, and the resulting ice cover time series match those that can be considered in situ ice observations by the USGS. For a time period of 151 days including freeze-up, two midwinter thawing and ice break-up events, high confidence ice maps show zero non-detections and one false ice detection. Ice maps also agree with observed locations and time periods of ice jams and warnings issued by the National Weather Service. Due to limited data, it is difficult to determine how accurately STC maps the spatial distribution of ice. Visual comparisons of ice maps generated by STC with Landsat8 and CRIOS show good agreement. Ice processes inferred from temperature, AFDD, river discharge magnitudes and estimates are also found to be in agreement with outputs of the STC algorithm.

Improved effective area coverage and, hence, reduced effective revisit time while the river bears ice is particularly relevant for river ice monitoring, both accurate and timely observations are needed. It is shown that a substantial portion of grid cells labeled by the Aqua cloud mask as cloudy can still be used to reasonably well infer information on river ice. The methodology presented herein can be applied to other platforms, as long as they have the appropriate resolution and bands. However, to apply the approach to other areas it is important to obtain a high quality land/water mask, re-evaluate thresholds to be used and possibly modify the algorithm logic. For instance, band 5 can be considered to better identify snow in areas where masking of the underlying land surface by snow is not as strong. The algorithm, its outputs and past data will be hosted at NOAA-CREST at the City College of New York. Ice maps are directly applicable for river ice monitoring as well as ice jam and flood forecasting. They may be useful to initialize numerical models such as HEC-RAS (ice module), to better estimate ensuing flood levels and severity. Ice maps may also be useful for studies related to climate, transportation, hydropower and environmental impacts.

Acknowledgements

The authors would like to thank Dr. Bill Rossow (CCNY) for his insights and useful suggestions with respect to the algorithm and the reviewers for their helpful comments. This work is supported by the National Oceanic and Atmospheric Administration (NOAA) under CREST grant #NA11SEC4810004. The views, opinions and findings contained in this report are those of the authors and should not be construed as an official NOAA or U.S. Government position, policy or decision.

References

Baker, N., 2011. Joint Polar Satellite System (JPSS) VIIRS Snow Cover Algorithm Theoretical Basis Document (ATBD).

Beltaos, S., Prowse, T.D., 2001. Climate impacts on extreme ice-jam events in Canadian rivers. Hydrol. Sci. J. 46 (1), 157–181 (http://doi.org/10.1.1.137.5497).

Chaouch, N., Temimi, M., Romanov, P., Cabrera, R., McKillop, G., Khanbilvardi, R., 2012. An automated algorithm for river ice monitoring over the Susquehanna River using the MODIS data. Hydrol. Process. 28 (1), 62–73. http://dx.doi.org/10.1002/hyp.9548.

EIJ, 2013. Earth Imaging Journal. Retrieved from http://eijournal.com/news/industry-insights-trends/yukon-river-ice-jam-causes-flooding (7/2016).

Hall, D.K., Riggs, G.A., 2007. Accuracy assessment of the MODIS snow products. Hydrol. Process. 21 (12), 1534–1547.

Hall, D.K., Riggs, G.A., Salomonson, V.V., DiGirolamo, N.E., Bayr, K.J., 2002. MODIS snow-cover products. Remote Sens. Environ. 83 (1), 181–194. http://dx.doi.org/10.1016/S0034-4257(02)00095-0.

Kraatz, S., Khanbilvardi, R., Devineni, N., 2015. Retrieval of river ice parameters for ice jam prediction with MODIS on the lower Susquehanna. Poster Presented at the 95th Annual Meeting of the American Meteorological Society, Phoenix, AZ.

Li, S., 2013. Development of an Integrated High Resolution Flood Product With Multi-source Data (Doctoral dissertation) George Mason University.

Maddux, B.C., Ackerman, S.A., Platnick, S., 2010. Viewing geometry dependencies in MODIS cloud products. J. Atmos. Ocean. Technol. 27 (9), 1519–1528.

Muhammad, P., Duguay, C., Kang, K.K., 2015. Monitoring Ice Break-up on the Mackenzie River Using MODIS Data.

Newsminer, 2013. Newsminer. Retrieved September 20, 2015, from http://www.newsminer.com/news/local_news/yukon-river-ice-jam-that-led-to-alaska-flooding-churns/article_c71f288c-c8a3-11e2-9e28-0019bb30f31a.html.

Pavelsky, T.M., Smith, L.C., 2004. Spatial and temporal patterns in Arctic river ice breakup observed with MODIS and AVHRR time series. Remote Sens. Environ. 93 (3), 328–338. http://dx.doi.org/10.1016/j.rse.2004.07.018.

Riggs, G.A., Hall, D.K., 2002, June. Reduction of cloud obscuration in the MODIS snow data product. 59th Eastern Snow Conference (Vol. 5, No. 7).

Riggs, G.A., Hall, D.K., 2004, June. Snow mapping with the MODIS Aqua instrument. Proceedings of 61st Eastern Snow Conference, pp. 9–11.

Rossow, W.B., Schiffer, R.A., 1999. Advances in understanding clouds from ISCCP. Bull. Am. Meteorol. Soc. 80 (11), 2261–2287. http://dx.doi.org/10.1175/1520-0477(1999)080<2261:AIUCFI>2.0.CO;2.

Satterwhite, M.B., Mitchell, H.J., Hemmer, T., Leckie, J.D., 2003. Field spectral signatures of snow, ice, and water. AeroSense 2003, pp. 528–537.

Sirguey, P., Mathieu, R., Arnaud, Y., 2009. Subpixel monitoring of the seasonal snow cover with MODIS at 250 m spatial resolution in the Southern Alps of New Zealand: methodology and accuracy assessment. Remote Sens. Environ. 113 (1), 160–181.

SRBC, 2015. SRBC fact sheet. Retrieved September 20, 2015, from http://www.srbc.net/pubinfo/docs/SRBGeneral 5_13 Updated.pdf.

Stefan, J., 1891. {Ü}ber die Theorie der Eisbildung, insbesondere {ü}ber die Eisbildung im Polarmeere. Ann. Phys. 278 (2), 269–286.

Stubenrauch, C.J., Rossow, W.B., Kinne, S., Ackerman, S., Cesana, G., Chepfer, H., et al., 2013. Assessment of global cloud datasets from satellites: project and database initiated by the GEWEX Radiation Panel. Bull. Am. Meteorol. Soc. 94 (7), 1031–1049. http://dx.doi.org/10.1175/BAMS-D-12-00117.1.

Tselioudis, G., Rossow, W., Zhang, Y., Konsta, D., 2013. Global weather states and their properties from passive and active satellite cloud retrievals. J. Clim. 26 (19), 7734–7746. http://dx.doi.org/10.1175/JCLI-D-13-00024.1.

Vermote, E.F., Kotchenova, S.Y., Ray, J.P., 2011. MODIS Surface Reflectance User's Guide. MODIS Land Surface Reflectance Science Computing Facility Retrieved from http://modis-sr.ltdri.org/products/MOD09_UserGuide_v1_3.pdf.

Warren, S.G., 1982. Optical Properties of Snow.

White, K.D., Eames, H.J., 1999. CRREL Ice Jam Database.

Wilson, A.M., Parmentier, B., Jetz, W., 2014. Systematic land cover bias in Collection 5 MODIS cloud mask and derived products—a global overview. Remote Sens. Environ. 141, 149–154.

Zubov, N.N., 1963. Arctic Ice. Naval Oceaonoagraphic Office, Washington DC.